PHILOSOPHICAL TRANSACTIONS A

royalsocietypublishing.org/journal/rsta

A practical method for estimating coupling functions in complex dynamical systems

Isao T. Tokuda[1], Zoran Levnajic[2] and Kazuyoshi Ishimura[1]

[1]Department of Mechanical Engineering, Ritsumeikan University, Kusatsu, Japan

[2]Complex Systems and Data Science Lab, Faculty of Information Studies in Novo Mesto, Novo Mesto, Slovenia

ITT, 0000-0001-6212-0022

Review

Check for updates

Cite this article: Tokuda IT, Levnajic Z, Ishimura K. 2019 A practical method for estimating coupling functions in complex dynamical systems. *Phil. Trans. R. Soc. A* **377**: 20190015. http://dx.doi.org/10.1098/rsta.2019.0015

Accepted: 2 September 2019

One contribution of 14 to a theme issue 'Coupling functions: dynamical interaction mechanisms in the physical, biological and social sciences'.

Subject Areas:
complexity

Keywords:
coupling function, phase dynamics, parameter estimation

Author for correspondence:
Isao T. Tokuda
e-mail: isao@fc.ritsumei.ac.jp

A foremost challenge in modern network science is the inverse problem of reconstruction (inference) of coupling equations and network topology from the measurements of the network dynamics. Of particular interest are the methods that can operate on real (empirical) data without interfering with the system. One such earlier attempt (Tokuda *et al.* 2007 *Phys. Rev. Lett.* **99**, 064101. (doi:10.1103/PhysRevLett.99.064101)) was a method suited for general limit-cycle oscillators, yielding both oscillators' natural frequencies and coupling functions between them (phase equations) from empirically measured time series. The present paper reviews the above method in a way comprehensive to domain-scientists other than physics. It also presents applications of the method to (i) detection of the network connectivity, (ii) inference of the phase sensitivity function, (iii) approximation of the interaction among phase-coherent chaotic oscillators, and (iv) experimental data from a forced Van der Pol electric circuit. This reaffirms the range of applicability of the method for reconstructing coupling functions and makes it accessible to a much wider scientific community.

This article is part of the theme issue 'Coupling functions: dynamical interaction mechanisms in the physical, biological and social sciences'.

1. Introduction

Complex networks are representations of complex systems, where nodes (vertices) represent the system's units and links (edges) represent the interactions

THE ROYAL SOCIETY PUBLISHING

among those units [1–4]. The functioning of a real network is a cumulative effect of its structure (topology of connections among nodes/units) and dynamics (interactions/relationships among these nodes) [3,4]. Hence, in models of real networks, nodes are often assumed to be (simple) systems with their inherent dynamics, whereas links mediate the dynamical coupling between the connected pairs of nodes. Using this paradigm, network science has made valuable contributions to all scientific disciplines that involve systems composed of many units, including biology, neuroscience, sociology, economics, etc. [1–6].

To really grasp the functioning of a real network, we need information on both its structure and its dynamics. The inverse problem of reconstructing (or inferring) this information from the empirical data is a foremost challenge in modern network science. Namely, understanding the inner connectivity patterns of real networks not only enables us to grasp their operations, but also helps in controlling and predicting their behaviour [7–19].

The problem of network reconstruction can be seen as composed of two parts. The first part is the reconstruction of network topology, where one tries to learn which pairs of nodes are connected and which are not. This can (in some cases) be done separately from the second part of the problem, which is the reconstruction of the coupling functions that dictate how the connected nodes interact. Of course, two parts of the problem are inherently related, but which one to tackle first depends on what data are available, what assumptions can be reasonably made about the system, and what exactly we wish to learn.

Numerous reconstruction methods have been proposed over the last decade, both in physics [7–21] and in computer science literature [16,22–30]. While some methods tackle only one of the two above-mentioned parts of the problem [10], other methods seek to address both parts at the same time. In physics literature, special emphasis is put on the methods aimed at oscillatory systems as the most researched paradigm of collective dynamics. This includes methods focused on either topology, coupling functions or both [7,8,10,18].

On a somewhat different front, research efforts have been devoted to the problem of estimation of phase variables and phase equations from the data [7,11,31–38]. Namely, isolated units in many real systems exhibit oscillatory nature, in the sense that they can be well approximated as limit-cycle oscillators (oscillator whose dynamics after transients reduces to periodic or quasi-periodic orbit). Researchers showed that, even if the oscillatory behaviour is very stochastic, there are robust ways to extract a well-defined phase variable for each network node, and hence reconstruct the phase equations that describe the system dynamics. This paradigm found applications in diverse domain sciences, notably biology and neuroscience, where many systems have this nature. Estimating phase equations, however, is nothing but reconstructing coupling functions from data. While such a reconstruction approach is valid only in the approximation of phase variables, these methods require very little additional assumptions about the system. This means they can be almost immediately applied to empirical data [7,31,36,39–41].

For a system of phase equations, a standard way to construct the coupling function is to measure the phase sensitivity function of an individual oscillator element and obtain the coupling function by averaging method that computes the amount of phase shift induced through interaction with another oscillator element [42]. However, a precisely measured phase sensitivity function is not always accessible, since it requires application of external perturbations to an individual oscillator, which cannot always be isolated from the rest of the system [43–52].

On the other hand, as a non-invasive approach, the coupling function can be inferred directly from time-trace data measured from coupled oscillators [7,31–36,38,40,41]. One of them is a method by Tokuda *et al.* [31]: this approach used a multiple shooting method to realize robust parameter estimation of the coupling functions. The multiple shooting provides a general framework for fitting ordinary differential equations to recorded time-trace data. It is applicable to any system, where the dynamics of individual nodes can be approximated as those of limit-cycle oscillators, yielding both oscillators' natural frequencies and coupling functions between them (phase equations). Most importantly, the method was actually shown to operate very well with the data from a real experiment, which highlights its potential for practical use for physics problems and otherwise [31,40,53].

The contribution of the present paper is twofold. First, we review this method in a way that is understandable and approachable to communities outside physics. With this, we hope to make our method more useful to fields such as biology and neuroscience, for which it was originally intended. Second, we show and discuss applications of this method, specifically: (i) we use the estimated coupling function for detecting the connectivity of oscillator networks, (ii) the method is extended to inference of the phase sensitivity function, which is vital for phase equations, (iii) the coupling function is estimated for coupled chaotic oscillators to demonstrate how well the phase model approximates chaotic phase synchronization, and (iv) using an experimental data from a system of Van der Pol electric circuits, we show how the method can be applied to real data.

The rest of the paper is organized as follows. In the next section, we review the original method in a comprehensive way. In §3, we discuss the problem of inferring the network connectivities. In §4, we present further applications mentioned above. In the last section, we discuss our findings and lay out perspectives for future work.

2. The original method

In this section, we describe the original method in a more comprehensive way than the original literature [31] and show how it works for the case of coupled FitzHugh–Nagumo oscillators.

(a) Multiple shooting method

Our approach is based on the multiple shooting method, which has been developed in physics and engineering to provide a general framework for fitting ordinary differential equations to recorded time series [54]. The methodology is applicable to a situation where the system equations are known *a priori*. When the equations and the recorded data are in a good quantitative agreement, unknown parameters of the system can be precisely estimated as follows.

We consider a nonlinear system

$$\dot{\boldsymbol{x}} = \boldsymbol{F}(\boldsymbol{p}, \boldsymbol{x}), \tag{2.1}$$

where $\boldsymbol{x}$, $\boldsymbol{p}$ and $\boldsymbol{F}$ represent state variables, parameters and autonomous dynamics of the system, respectively. The system may generate nonlinear dynamics such as limit cycles, torus, strange attractors and transient dynamics to these attractors. Equation (2.1) may describe a variety of systems of interest in science and engineering such as electric circuits and lasers. Empirical data consist of oscillators' states measured as $\{\boldsymbol{x}(n\Delta t)) : n = 1, \ldots, M\}$ (Δt: sampling time, M: data points). This corresponds to an experimental situation, in which the system state (e.g. current and voltage of electric circuits, laser, etc.) is fully recorded. Then the parameter values $\boldsymbol{p}$ that underlie the measurement data can be estimated by fitting the original equations (2.1) to the recording data. First, time evolution of the original equations (2.1) starting from an initial condition $\boldsymbol{x}(0)$ is denoted by $\boldsymbol{\phi}^t(\boldsymbol{x}(0), \boldsymbol{p})$. Then, at each sampling time $t = i\Delta t$, the equations must satisfy the boundary conditions: $\boldsymbol{x}((n+1)\Delta t) = \boldsymbol{\phi}^{\Delta t}(\boldsymbol{x}(n\Delta t), \boldsymbol{p})$. With respect to the unknown parameters $\boldsymbol{p}$, these nonlinear equations are solved by the generalized Newton method [55]. To compute the gradients $\partial\phi_i/\partial p$, which are needed for the Newton method, variational equations $(\mathrm{d}/\mathrm{d}t)(\partial\phi_i/\partial p_j) = \partial f_i/\partial p_j + \sum_{k=1}^{N}(\partial f_i/\partial\phi_k)(\partial\phi_k/\partial p_j)$ are solved simultaneously, where f_i represents ith equation of the original dynamics (2.1) as $\dot{x}_i = f_i(\boldsymbol{x}, \boldsymbol{p})$. The evolution function ϕ^t as well as the variational equations are integrated numerically, using whichever integration scheme (e.g. 4th-order *Runge–Kutta*). It has been shown that, when the equations and the experimental data are in good quantitative agreement, the unknown parameters can be precisely estimated for real-world systems including electric circuits and lasers. All steps in the above computational procedure can be realized relatively easily with standard programming knowledge.

(b) Problem and method

Equipped with the knowledge of multiple shooting method, we now explain in detail how it can be used for inferring the coupling functions. We begin by considering a network composed of interacting oscillator elements. In biology, such systems include a network of circadian cells in the suprachiasmatic nucleus [56], brain network composed of many spiking neurons [43,46], cardiac muscle cells in the heart [57], etc. In terms of nonlinear dynamics, such systems are described as a system of N coupled limit cycle oscillators:

$$\dot{\boldsymbol{x}}_i = \boldsymbol{F}_i(\boldsymbol{x}_i) + \frac{C}{N}\sum_{j=1, j\neq i}^{N} T_{i,j}\boldsymbol{G}(\boldsymbol{x}_i, \boldsymbol{x}_j). \tag{2.2}$$

Here, $\boldsymbol{x}_i$ and $\boldsymbol{F}_i$ $(i = 1, 2, \ldots, N)$ represent state variables and autonomous dynamics of the ith oscillator element, respectively. While $\boldsymbol{G}$ represents an interaction function between the ith and jth oscillators, the strength of their interaction is determined by the coupling constant C. The matrix $\{T_{i,j}\}$ describes connectivity between the oscillator elements. For simplicity, we suppose that the connection matrix is composed of zero-or-unity elements (i.e. $T_{i,j} = 0$ or 1). We assume that, without coupling (i.e. $C = 0$), individual systems (i.e. $\dot{\boldsymbol{x}}_i = \boldsymbol{F}_i(\boldsymbol{x}_i)$) generate periodic oscillations, after transients. Such closed trajectories in phase space are called *limit cycles*, which have intrinsic periods of τ_i. Equation (2.2) describes, to a good approximation, a variety of systems of interest in biology and neuroscience. Then the theory of phase reduction [58,59] states that, as far as the coupling strength C is weak enough, the network dynamics can be reduced to the following phase equations:

$$\dot{\theta}_i = \omega_i + \frac{C}{N}\sum_{j=1, j\neq i}^{N} T_{i,j}\boldsymbol{Z}(\theta_i)\boldsymbol{G}(\theta_i, \theta_j) = \omega_i + \frac{C}{N}\sum_{j=1, j\neq i}^{N} T_{i,j}H(\theta_j - \theta_i), \tag{2.3}$$

where θ_i represents phase of the ith oscillator and ω_i gives natural frequency of the ith oscillator (i.e. $\omega_i = 2\pi/\tau_i$). $\boldsymbol{Z}$ stands for phase sensitivity function (also called 'infinitesimal phase response curve'), which determines the amount of phase shift induced by the interaction $\boldsymbol{G}$ with other oscillators (we will here not go in the detail of how equation (2.3) is obtained; an interested reader can refer to [58–60]). By averaging approximation [59], which integrates one cycle of the phase sensitivity function $\boldsymbol{Z}$ with the interaction function $\boldsymbol{G}$, the coupling function is derived as $H(\theta_i - \theta_k) = (1/2\pi)\int_0^{2\pi} \boldsymbol{Z}(\theta_i + \theta')\boldsymbol{G}(\theta_i + \theta', \theta_k + \theta')\,\mathrm{d}\theta'$. Transformation of the original equations (2.2) and (2.3) provides a significant reduction in the system's dimensionality, in the sense that the original state variables $\boldsymbol{x}_i$, which can be high-dimensional, are represented only by the single-phase variable θ_i. This substantially simplifies the system's modelling and enables its identification in a straightforward fashion.

The individual oscillator states are simultaneously measured as $\{\xi_i(n\Delta t) = \eta(\boldsymbol{x}_i(n\Delta t)) : n = 1, \ldots, M\}_{i=1}^{N}$ (η: observation function, Δt: sampling time, M: data points). This corresponds to an experimental situation, under which states of individual oscillators (e.g. gene expression levels of individual cells, membrane potentials of neurons, etc.) are recorded simultaneously. Our purpose is to infer the phase equations from these measurement data under the conditions that the underlying system equations (2.2) are unknown.

The phase dynamics can be reconstructed via the following steps.

(i) From the measured data $\{x_i(t)\}$, phases are extracted as $\theta_i(t) = 2\pi k + 2\pi(t - t_k)/(t_{k+1} - t_k)$, where t_k represents the time, at which the ith signal takes its kth peak and $t_k \leq t < t_{k+1}$ [60]. Note that this method is limited to the case of simple waveform, where a single peak appears during one oscillation cycle.

(ii) Fit the phase equations:

$$\dot{\theta}_i = \tilde{\omega}_i + \frac{C}{N}\sum_{j=1}^{N} \tilde{T}_{i,j}\tilde{H}(\theta_j - \theta_i) \tag{2.4}$$

to the phase data $\{\theta_i(t)\}$. Here, $\{\tilde{\omega}_i\}$ represent approximate values for the natural frequencies. The coupling function $\tilde{H}$, which is in general nonlinear and periodic with respect to 2π, is approximated by a *Fourier* series of pre-selected order D as $\tilde{H}(\Delta\theta) = \sum_{j=1}^{D} a_j \sin j\Delta\theta + b_j(\cos j\Delta\theta - 1)$. For simplicity, we consider a specific type of coupling, under which the interaction disappears as the phase difference becomes zero, i.e. $\tilde{H}(0) = 0$. This type of coupling arises quite often in diffusively coupled oscillator networks [59,61]. (Although general coupling can be also considered, more than one dataset associated with different coupling strength is required to avoid parameter redundancy. As a simplified demonstration, this study deals with this specific coupling.)

The unknown parameters $\boldsymbol{p} = \{\tilde{\omega}_i, a_j, b_j\}$ are now estimated by the above described multiple-shooting method (the connection matrix $\tilde{T}_{i,j}$ and the coupling strength $C = 0$ are supposed to be known here).

(iii) To avoid over-fitting of the coupling function, cross-validation is used to determine the optimal number of *Fourier* components D [62]. We divide the measurement data into two parts. For the first half data, the parameter values $\boldsymbol{p}$ are estimated. Then, the estimated parameters are applied to the latter half data and measure the error $e_{cv} = \sum_n |\boldsymbol{\theta}((n+1)\Delta t) - \boldsymbol{\phi}^{\Delta t}(\boldsymbol{\theta}(n\Delta t), \boldsymbol{p})|^2$, where $\boldsymbol{\phi}^{\Delta t}(\boldsymbol{\theta}(n\Delta t), \boldsymbol{p})$ represents Δt-time further state of the phase dynamics (2.4) starting from an initial condition $\boldsymbol{\theta}(n\Delta t)$. The order number D providing the minimum error is considered as the optimum.

(c) Application to coupled FitzHugh–Nagumo oscillators

To illustrate how the method described above works, we apply the multiple shooting to a prototypical example of weakly coupled limit cycle oscillators. In the original study [31], coupled Rössler oscillators were analysed. As another challenging example, which has a more complex shape of coupling function due to the nature of relaxation oscillations, we consider the following network of FitzHugh–Nagumo (FHN) oscillators [63,64]:

$$\dot{v}_i = \alpha_i \left(v_i - \frac{v_i^3}{3} - w_i + I \right) + \frac{C}{N} \sum_{j=1}^{N} T_{i,j}(x_j - x_i) \tag{2.5}$$

and

$$\dot{w}_i = \alpha_i \epsilon (v_i + a - b y_i), \tag{2.6}$$

where $i = 1, \ldots, N$. The system of FitzHugh–Nagumo oscillators can be seen as a simple model for interacting neurons. Under the parameter setting of $a = 0.7$, $b = 0.8$, $\epsilon = 0.08$, $I = 0.8$, individual FHN oscillators (without coupling $C = 0$) gives rise to limit cycles of the slow–fast type. Inhomogeneity parameters, which control natural periods of the individual oscillators, were set as $\alpha_i = 1 + (i-1)\Delta\alpha$ ($i = 1, \ldots, N$), where $\alpha_i = 1$ yields a natural oscillation period of 36.5.

We started with the case of $N = 16$. We consider all-to-all coupling matrix ($T_{i,j} = 1$). The level of inhomogeneity was set to $\Delta\alpha = 0.01$. The multivariate data $\{x_i(t)\}_{i=1}^{16}$ were recorded at a coupling strength of $C = 0.01$, which is in a non-synchronized regime. The sampling interval was set to be $\Delta t = 0.004$. Then, the phases $\{\theta_i(t)\}$ were extracted and down-sampled to a sampling interval of $\Delta t = 1000 \cdot 0.004$. Total of 500 data points have been collected for the parameter estimation. As an initial condition, the unknown parameter values were all set to be zero, i.e. $\tilde{\omega}_i = 0$, $a_j = b_j = 0$. The 500 data were divided into 250 and 250, which were used for the parameter estimation and the cross-validation error e_{cv}, respectively. By varying the number of *Fourier* components from $D = 1$ to $D = 10$, the optimal value was found to be $D = 7$ by the cross-validation test.

The coupling function $\tilde{H}(\Delta\theta)$ estimated by the present method is in good agreement with the one computed by the adjoint method [65] (figure 1*a*). The error-bars were computed from inverse of the Hessian matrix of the squared error function, under the assumption that the phase data contain uncorrelated observational noise [66]. The estimated natural frequencies are distributed

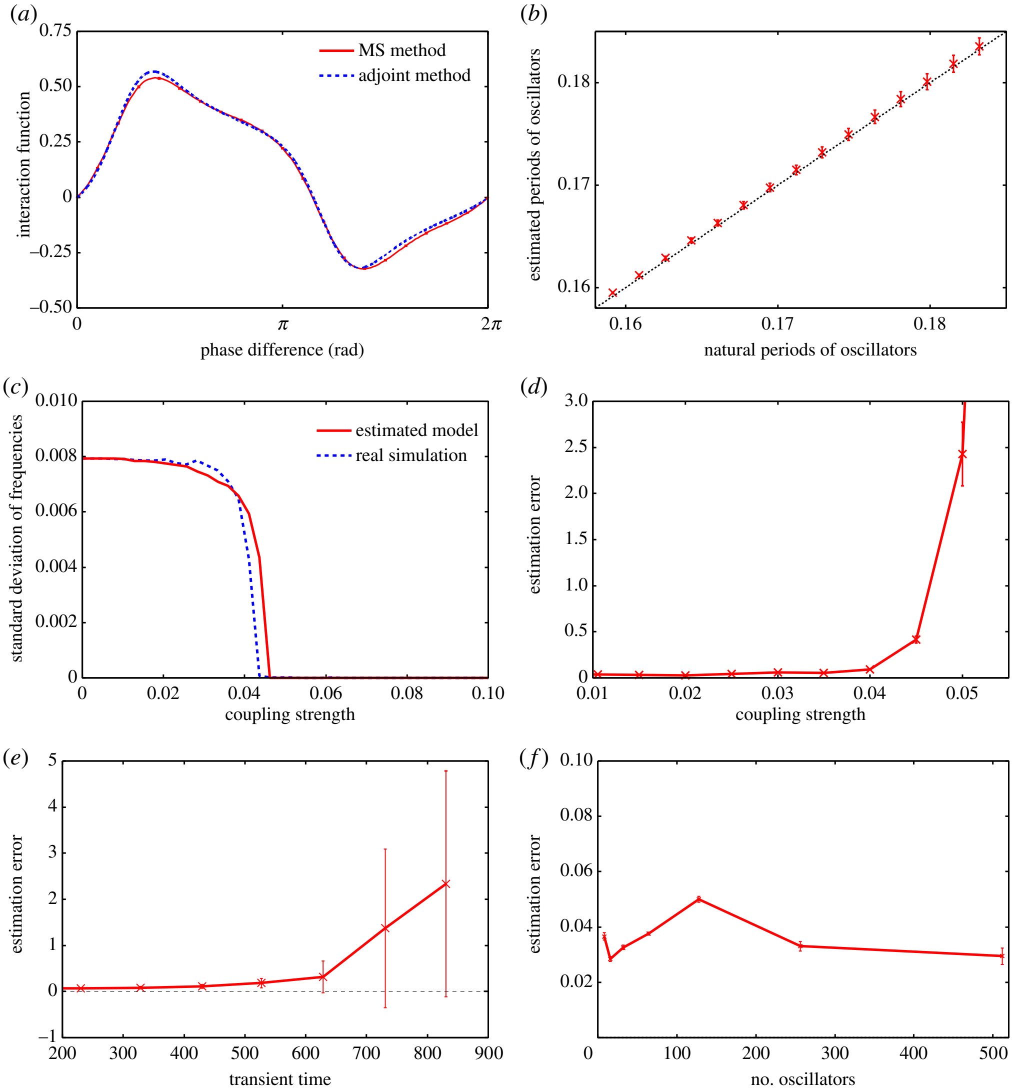

Figure 1. Results for a network of $N = 16$ FHN oscillators. (*a*) Coupling functions $\tilde{H}(\Delta\theta)$ estimated by the present method (solid red line) and the adjoint method (dashed blue line). (*b*) Estimated natural frequencies (ordinate) $\{\omega_i\}_{i=1}^{16}$ of FHN oscillators versus those obtained from non-coupled simulation (abscissa). (*c*) Synchronization diagrams of the estimated model (solid red line) and the original coupled oscillators (dashed blue line). (*d*) Dependence of estimation error on the coupling strength C used to generate multivariate data. The estimation error e is defined as the deviation of the estimated coupling function from the one computed by the adjoint method. (*e*) Dependence of the estimation error on the transient time, after which the multivariate data were sampled. The coupling strength was set to $C = 0.05$. (*f*) Dependence of the estimation error on the number of oscillators N. (Online version in colour.)

on a diagonal line with the true frequencies obtained from simulations of the individual (isolated) FHN oscillators (figure 1*b*). Using the estimated phase equations, a synchronization diagram of the original coupled FHN oscillators can be recovered, where the onset of synchronization was predicted at $C = 0.046$, which is very close to the real onset of $C = 0.044$ (figure 1*c*).

Next, we show how the estimation depends upon the problem setting. The primary factor that influences the estimation results is the coupling strength C used to generate the time series. Figure 1*d* shows dependence of estimation error on the coupling strength. The estimation error

e_{cf} is evaluated as deviation of the estimated coupling function $\tilde{H}_s(\Delta\theta)$ from the one $\tilde{H}_p(\Delta\theta)$ estimated by the adjoint method, i.e.

$$e_{\text{cf}} = \frac{\sqrt{\int_0^{2\pi} \{\tilde{H}_s(\Delta\theta) - \tilde{H}_p(\Delta\theta)\}^2 \, \mathrm{d}\Delta\theta}}{\sqrt{\int_0^{2\pi} \{\tilde{H}_p(\Delta\theta) - \langle \tilde{H}_p \rangle\}^2 \, \mathrm{d}\Delta\theta}}, \tag{2.7}$$

where the denominator represents normalization factor and $\langle \tilde{H}_p \rangle = (1/(2\pi)) \int_0^{2\pi} \tilde{H}_p(\Delta\theta) \, \mathrm{d}\Delta\theta$. As the coupling strength is located close to the onset of synchronization, the estimation error increases significantly (figure 1*d*). Under the synchronized state, phase differences between the oscillators do not change in time $\Delta\theta = \text{const.}$, providing no information about the phase interaction. Increase in estimation error due to synchronized data is therefore reasonable.

Even in a synchronized regime, the coupling function can be recovered from transient data, during which phase differences evolve (transient data often reveals far more information about the underlying system, since it is recorded before the system 'settled' into its dynamical equilibrium). To show this, the multivariate data were recorded after discarding only a short duration of transient process that starts from a random initial condition. Transient data (time interval of 40) were collected before the system reached the final synchronized state. Twenty sets of such data were used for the parameter estimation. Figure 1*e* shows dependence of the estimation error on the transient duration. Note that the coupling strength is set to $C = 0.05$, which is in a synchronized regime. Although the error increases as the transient duration is increased, relatively good estimation was realized for a short transient time. This suggests that, even if the system is in synchrony with a moderate coupling, application of perturbation that kicks the system out of synchrony is an efficient way of inferring the underlying phase dynamics.

Figure 1*f* shows dependence of the estimation error on the network size N, varied from 8 to 512. The level of inhomogeneity was set to $\Delta\alpha = 0.16/N$. The multivariate data $\{y_i(t)\}_{i=1}^N$ were recorded at a coupling strength of $C = 0.02$, which corresponds to non-synchronized regime. Other settings were the same as those in the case of $N = 16$. Surprisingly, the estimation error remains at a low level. Even for $N = 512$, the coupling function $\tilde{H}(\Delta\theta)$ has been precisely estimated, while the estimated natural frequencies $\{\omega_i\}_{i=1}^{512}$ are consistent with those obtained from the non-coupled simulations. This suggests that the system size does not impose a major limit on the estimation of phase dynamics as far as the data contain non-synchronized phase information.

Although the coupling function has been reliably estimated for networks with all-to-all connections ($T_{i,j} = 1$), the estimation error may increase when oscillators are heterogeneously connected to each other. We deal with such situations in the next section.

3. Application to network inference

Although we have dealt with the case that all oscillator elements are connected to all the others in the previous section, heterogeneous connections are more common in nature and engineering. As another challenge of our technique [53], this section discusses a problem of inferring connectivity of the oscillator network from the measured time series. Numerous approaches have been proposed up to date using information transfer [67], mutual predictability [68], recurrence properties [69], permutation-based asymmetric association measure [70], index for partial phase synchronization [71–73] and graph theory [74]. Response properties of the network dynamics to external stimuli have been also exploited [8,75]. For weakly coupled limit cycle oscillators, to which phase reduction is applicable, the phase modelling approach is again quite effective for detecting the network topology [11,53,76–78].

In our approach [53], the multiple-shooting method is again applied to fit the phase equations (2.4) to the phase data $\{\theta_i(t)\}$. The fitting procedure is the same as before except that the connection matrix is estimated as the unknown parameters $\boldsymbol{p} = \{\tilde{T}_{i,j}\}$. For simplicity, the coupling function $\tilde{H}$ and the natural frequencies $\{\omega_i\}_{i=1}^N$ of the oscillator elements were assumed to be known (the general case that both coupling function and connection matrix are unknown has

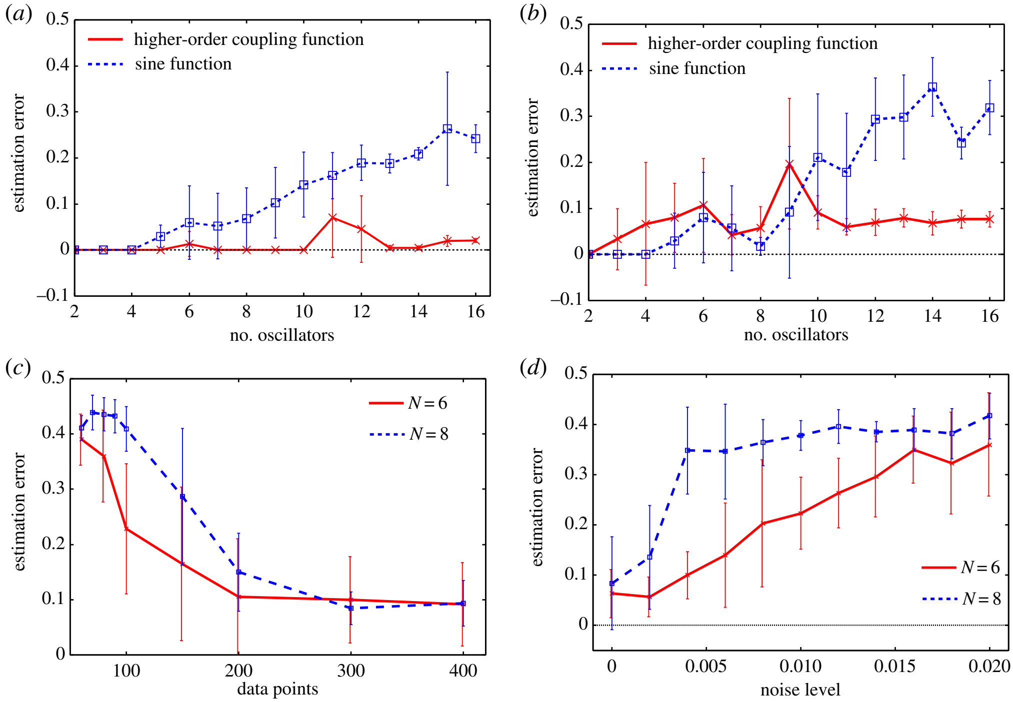

Figure 2. Estimation errors of the network connectivity. (*a*) Percentage of non-connected pairs of oscillators is 20%. The coupling function is composed of higher-order ($D = 5$) *Fourier* components in solid red line, while it is based on a simple sine function in dashed blue line. (*b*) Percentage of non-connected pairs of oscillators is 40%. (*c*) Dependence of the estimation error on data length. Percentage of non-connected pairs of oscillators is 40%, while number of the oscillators is set to $N = 6$ (solid red line) and $N = 8$ (dashed blue line). (*d*) Dependence of the estimation error on noise level σ, where *Gaussian* noise $N(0, (2\pi\sigma)^2)$ is added to the phase data. Percentage of the non-connected pairs of oscillators is 40%, while number of the oscillators is set to $N = 6$ (solid red line) and $N = 8$ (dashed blue line). (Online version in colour.)

been dealt with in the previous study [53]). As coefficients $\{a_j, b_j\}$ for the coupling function, the ones estimated in the previous section were used. Natural frequencies $\{\omega_i\}_{i=1}^{N}$ were also obtained from the simulations of non-coupled original equations.

As the target system, the network of FHN oscillators (2.5) and (2.6) were studied. For a network of four ($N = 4$) oscillators, two defects were introduced to the connection matrix as $T_{3,1} = T_{4,1} = 0$ (here, *defect* means that one oscillator is not connected to another). The level of inhomogeneity was set to $\Delta\alpha = 0.04$, whereas the coupling strength was $C = 0.02$, i.e. in a non-synchronized regime. As in the previous section, a total of 500 data points (sampling time: 4) have been collected. By the multiple-shooting method, the connection matrix was estimated as follows.

$$\begin{pmatrix} & \tilde{T}_{1,2} & \tilde{T}_{1,3} & \tilde{T}_{1,4} \\ \tilde{T}_{2,1} & & \tilde{T}_{2,3} & \tilde{T}_{2,4} \\ \tilde{T}_{3,1} & \tilde{T}_{3,2} & & \tilde{T}_{3,4} \\ \tilde{T}_{4,1} & \tilde{T}_{4,2} & \tilde{T}_{4,3} & \end{pmatrix} = \begin{pmatrix} & 1.11 \pm 0.01 & 1.08 \pm 0.01 & 1.06 \pm 0.01 \\ 1.06 \pm 0.02 & & 1.04 \pm 0.02 & 0.97 \pm 0.01 \\ -0.02 \pm 0.01 & 1.05 \pm 0.01 & & 1.03 \pm 0.01 \\ 0.04 \pm 0.01 & 0.98 \pm 0.01 & 1.03 \pm 0.01 & \end{pmatrix}.$$

We see that the two defects ($\tilde{T}_{3,1}$, $\tilde{T}_{4,1}$) were precisely identified as small values, whereas other matrix elements pointed to almost unity.

For comprehensive analysis, the connection matrices with randomly generated defects were estimated for variable network size from $N = 2$ to $N = 16$. For our analysis, the estimation error was evaluated as $e_{cm} = (1/N(N-1)) \sum_{i=1}^{N} \sum_{j=1, j\neq i}^{N} |\check{T}_{i,j} - T_{i,j}|$, where the estimated connectivity was digitized as $\check{T}_{i,j} = 0$ for $\tilde{T}_{i,j} < 0.5$ and $\check{T}_{i,j} = 1$ otherwise. For each setting of the network size, five instances of connection matrices $\{T_{i,j}\}$ were randomly generated and the average and the standard deviation of the estimation errors were plotted in figure 2. Panels (*a*) and (*b*) correspond to the cases that defect ratios (i.e. percentage of zero elements in the connection matrix) are 20% and 40%, respectively. For variable network sizes, the estimation errors $e_{\rm cm}$ are almost zero except $N = 11, 12$ in the case of low defect ratio. Although the errors increase for high defect ratio, their overall level is less than 0.2.

To examine the effect of coupling function, the connection matrices were also estimated by using a simple sine as the coupling function, i.e. $\tilde{H}(\Delta\theta) = a_1 \sin \Delta\theta$. For small networks, the difference was not large between the precisely estimated (higher-order) coupling function (red solid line) and the simple sine function (blue dotted line). However, as the network size increases, the estimation error increases much more rapidly in the sine function than in the higher-order coupling function. This indicates that, for reliable detection of the connectivities, precisely estimated coupling function is of significant importance.

In figure 2*c*, dependence of the network inference on data length M is indicated. For network sizes of $N = 6$ and $N = 8$, we have varied the data length and studied how it affected the estimation results of the network connectivity. The defect ratio was set to 40%. The network inference was reliable for data length longer than 200 points (i.e. about 20 cycles). For shorter data length, the estimation error gradually increased. It is therefore crucial to use enough data length for precisely detecting the network connectivity.

Figure 2*d* shows dependence of the network inference on *Gaussian* noise $N(0, (2\pi\sigma)^2)$ added to the phase data. The defect ratio and the data length were set to 40% and $M = 400$, respectively. The estimation error increased gradually as the noise level was increased, where $\sigma = 0.5\%$ and $\sigma = 2\%$ of phase noises caused severe damage to the network inference for system sizes of $N = 8$ and $N = 6$, respectively. This suggests that our estimation technique is rather sensitive to the phase noise and, for reliable estimation of the connection matrix, phase information should be accurately extracted from the observed time series.

4. Further applications

In this section, we discuss further applications of the multiple-shooting technique.

(a) Inferring phase sensitivity function

First, we apply the multiple-shooting method to the estimation of phase sensitivity function $Z(\theta)$. The phase sensitivity function $Z(\theta)$ plays a vital role in the studies of coupled oscillators, since it describes one of the most fundamental properties of the oscillator element [58–60]. Numerous approaches have been proposed to estimate the phase sensitivity function from experimental data [43–52]. As an extension of our technique, the phase sensitivity function can be recovered from the coupling function [79]. As described earlier in the averaging approximation [59], the coupling function is given by a convolution of the phase sensitivity function $Z(\theta)$ and the input waveform $G(\theta)$ as $H(\theta) = (1/2\pi)\int_0^{2\pi} Z(\psi)G(\theta + \psi)\,{\rm d}\psi = (Z{*}G)(\theta)$. It is straightforward to recover the phase sensitivity function by the spectral deconvolution [80]. Namely, in a frequency domain, the phase sensitivity function is given as $\hat{Z}(\omega) = \hat{H}(\omega)/\hat{G}(\omega)$, where $\hat{Z}(\omega)$, $\hat{H}(\omega)$ and $\hat{G}(\omega)$ represent *Fourier* transforms of Z, H and G, respectively. Inverse *Fourier* transform of $\hat{Z}(\omega)$ yields the phase sensitivity $Z(\theta)$. Figure 3*a* shows phase sensitivity function (solid red line) obtained by the deconvolution of the coupling function estimated from coupled FHN oscillators ($N = 16$) in §2. Compared with the one computed by the adjoint method [65] (dashed blue line), the estimated function is somewhat deviated from the true curve. We consider that, due to the averaging effect, where the effect of input signal is averaged over one oscillation cycle, information on the spontaneous phase response has been lost.

To improve the situation, the phase sensitivity can be estimated more directly by using the Winfree formula [58] as follows. For simplicity, we consider a single phase oscillator receiving lth external force $G_l(t)$ $(l = 1, 2, \ldots, L)$:

$$\dot{\theta}_l = \omega + \tilde{Z}(\theta_l)G_l(t), \tag{4.1}$$

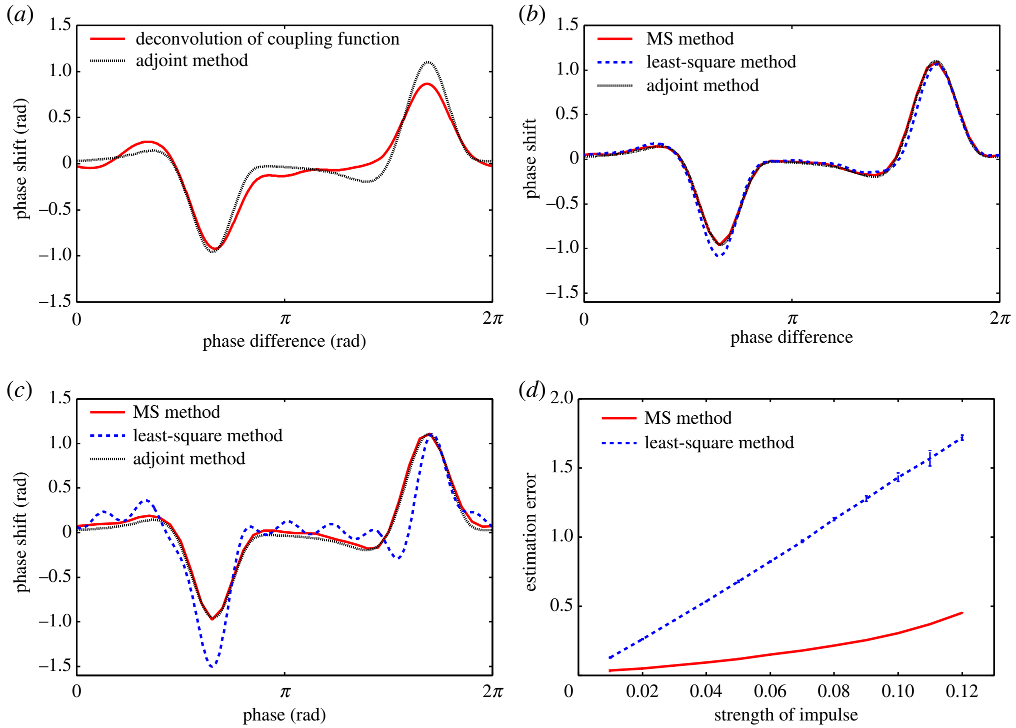

Figure 3. (*a*) Phase sensitivity function Z (solid red line) obtained by deconvolution of the coupling function estimated in figure 1*a*. Compared is the estimate by the adjoint method (dotted black line). (*b*,*c*) Phase sensitivity functions Z obtained by MS method (solid red) and the least-square method (dashed blue line). Strength of the impulse is $E = 0.01$ in (*b*) and $E = 0.04$ in (*c*). (*d*) Dependence of the estimation errors e of MS method (solid red line) and least-square method (dashed blue line) on strength E of the impulses injected to the FHN oscillator. (Online version in colour.)

where θ_l and ω represent phase and natural frequency of the oscillator. Without loss of generality, the initial phase can be set to zero (i.e. $\theta_l(0) = 0$). The external force $G_l(t)$ is typically composed of a short pulse, which lasts within one oscillator cycle of $T = 2\pi/\omega$. The phase sensitivity function $\tilde{Z}$ is described in terms of a *Fourier* series as $\tilde{Z}(\theta) = c_0 + \sum_{j=1}^{D} c_j \sin j\theta + d_j \cos j\theta$. The unknown coefficients $\boldsymbol{p} = \{c_j, d_j\}$ can be estimated by the multiple-shooting method in a similar manner as the estimation of coupling function. Given the external force $G_l(t)$, the phase oscillator model (4.1) can be integrated as $\phi^T(\theta_l(0), G_l, \boldsymbol{p})$. The parameters $\boldsymbol{p}$ can be optimized in such a way that the phase model (4.1) satisfies the boundary conditions: $\theta_l(T) = \phi^T(\theta_l(0), G_l, \boldsymbol{p})$, where $\theta_l(T)$ represents the oscillator phase observed at $t = T$.

Below, we compare the performance of the multiple-shooting method with that of least squares as the standard method of estimating the phase sensitivity function [43,46]. Here, the phase model (4.1) is integrated as

$$\int_0^T \mathrm{d}\theta_l = \int_0^T \omega\,\mathrm{d}t + \int_0^T \tilde{Z}(\theta_l) G_l(t)\,\mathrm{d}t$$

and

$$\theta_l(T) - \theta_l(0) - 2\pi = \int_0^T \tilde{Z}(\omega t) G_l(t)\,\mathrm{d}t,$$

where the oscillator phase is approximated as $\theta_l(t) \approx \omega t$ under the assumption that the external force $G_l(t)$ is weak in equation (4.1). By expanding the external force into *Fourier* series as $G_l(t) =$

$g_{l,0} + \sum_{j=1}^{D} g_{l,j} \sin j\omega t + h_{l,j} \cos j\omega t$, we obtain

$$M\mathbf{p} = \mathbf{D},$$

where

$$M = \begin{bmatrix} g_{1,0}/2 & g_{1,1} & h_{1,1} & g_{1,2} & h_{1,2} & \cdots & g_{1,D} & h_{1,D} \\ g_{2,0}/2 & g_{2,1} & h_{2,1} & g_{2,2} & h_{2,2} & \cdots & g_{2,D} & h_{2,D} \\ \vdots & \vdots & \vdots & \vdots & \vdots & \vdots & \vdots & \\ g_{L,0}/2 & g_{L,1} & h_{L,1} & g_{L,2} & h_{L,2} & \cdots & g_{L,D} & h_{L,D} \end{bmatrix}, \quad \mathbf{p} = \begin{bmatrix} c_0 \\ c_1 \\ d_1 \\ \vdots \\ c_D \\ d_D \end{bmatrix}, \quad \mathbf{D} = \begin{bmatrix} \Delta\theta_1 \\ \Delta\theta_2 \\ \vdots \\ \Delta\theta_L \end{bmatrix}.$$

$\Delta\theta_l = \theta_l(T) - \theta_l(0)$ represents phase shift induced by the lth external force $G_l(t)$. The unknown coefficients $\boldsymbol{p}$ can be obtained as $\boldsymbol{p} = DM^{-1}$.

We apply the two methods to a single FHN oscillator that receives 400 random impulses (stimulus duration: $\tau = 20$, stimulus strength: $V = 0.01, 0.02, \ldots, 0.12$) as external forcing $G(t)$. Parameter values of the FHN oscillator and the sampling time interval were set to be the same as those in the previous sections. For simplicity, natural frequency ω and the external signal $G(t)$ were assumed to be known. The number of the *Fourier* components was set to $D = 10$. The integration time was set to $T = 150$. For impulse strength of $E = 0.01$ and $E = 0.04$, the estimated phase sensitivity functions are drawn in figure 3*b*,*c*, respectively. In both panels (*b*) and (*c*), estimation results of the multiple shooting method (solid red lines) are consistent with those of the adjoint method [65]. The least-square method (dashed blue line), on the other hand, recovered the phase sensitivity function faithfully for a small impulse strength in (*b*). The estimate is, however, deviated from the other two curves for a large impulse strength in (*c*). In fact, as the impulse strength is increased, the estimation error increases much more rapidly in the least-squares method (dashed blue line) than the multiple shooting method (solid red line) (figure 3*d*). The least-squares method [43,46] assumes that phase of the oscillator evolves linearly in time according to the natural frequency. This approximation is effective as far as the external force is weak. If stronger perturbations are applied, inducing non-small phase shifts, this approximation increases the estimation error. The multiple-shooting method, on the other hand, takes into account the phase shift induced by the external perturbations by faithfully integrating the phase equation (4.1). The estimation error has been therefore reduced by the multiple-shooting method.

(b) Chaotic phase synchronization

Next we show how the estimated coupling function can be used for modelling chaotic phase synchronization [81]. It has been known that phases of chaotic oscillators can be synchronized with each other, while their amplitudes remain irregular and uncorrelated. Especially for phase-coherent chaos, in which rotation centre can be well defined, the phase dynamics can be approximated as $\dot{\theta} = \omega + \Gamma(A)$, where $\Gamma(A)$ represents frequency modulation, which depends upon oscillation amplitude A [81]. For chaotic amplitude A, the term $\Gamma(A)$ can be regarded as an effective noise. In many phase-coherent systems such as the Rössler equations [82], amplitude-dependent frequency modulation is very small, so the noise term $\Gamma(A)$ is negligible. Phase dynamics of such a chaotic attractor become very similar to those of limit cycle oscillators.

To extract phase-interaction between chaotic oscillators, we consider two coupled Rössler equations [82]:

$$\dot{x}_{1,2} = -\alpha_{1,2} y_{1,2} - z_{1,2},$$

$$\dot{y}_{1,2} = \alpha_{1,2} x_{1,2} + 0.15 y_{1,2} + C(y_{2,1} - y_{1,2})$$

and

$$\dot{z}_{1,2} = 0.2 + z_{1,2}(x_{1,2} - 7).$$

Each Rössler oscillator gives rise to chaotic dynamics without coupling $C = 0$. The inhomogeneity parameters were set as $\alpha_{1,2} = 1 \mp 0.01$, which yield average oscillation periods of 6.06 and 5.94,

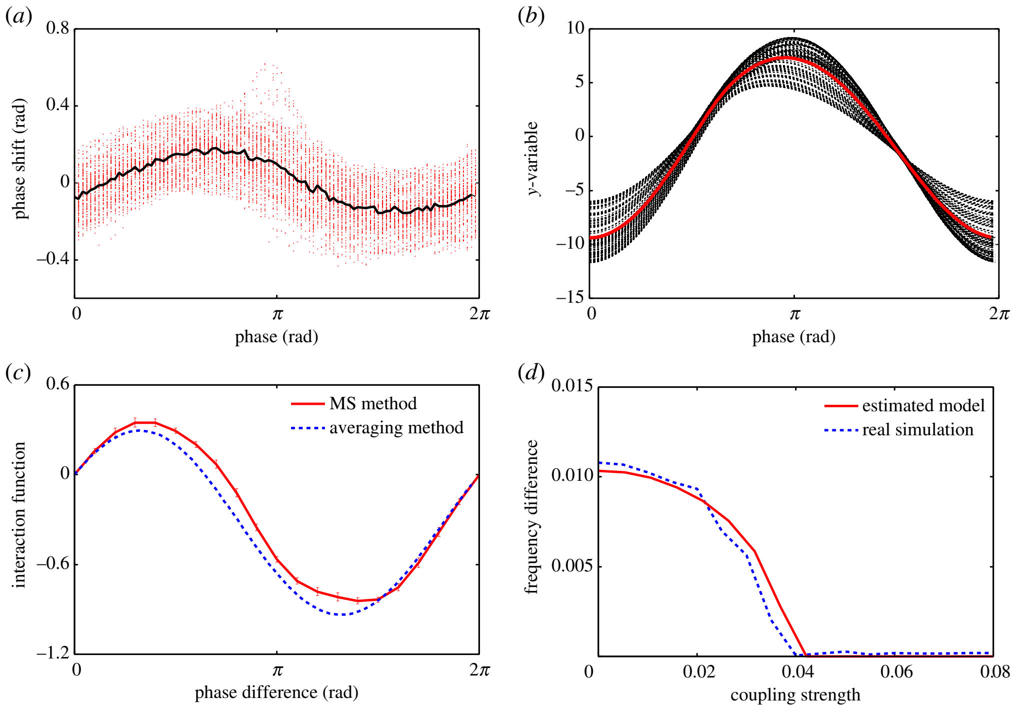

Figure 4. (*a*) Phase responses of chaotic dynamics observed from Rössler equations. By applying an impulse at variable phases, the phase shifts were measured as the difference in timing between the following peak of *y*-variable and the one expected from the average oscillation period. Bold black line represents the averaged phase response. (*b*) Waveforms of *y*-component of the Rössler equations. Bold red line represents the averaged waveform. (*c*) Coupling functions $\tilde{H}(\Delta\theta)$ estimated by the present method (solid red line) and one (dashed blue line) obtained as the convolution of averaged phase response curve and the averaged waveform. (*d*) Synchronization diagram of the estimated phase model (solid red line) and the original coupled Rössler equations (dashed blue line). (Online version in colour.)

respectively. The bivariate data $\{y_i(t)\}_{i=1}^{2}$ were simulated under coupling strength of $C = 0.02$, which corresponds to the non-synchronized regime. The sampling interval was set to be $\Delta t = 0.08$ for the extraction of the phases $\{\theta_i(t)\}$. Then, to apply the multiple-shooting method, the data have been down sampled to $\Delta t = 1000{\cdot}0.08$ and a total of 2000 data points were collected. The data were divided into 1000 and 1000 points, which were used for the parameter estimation and the cross-validation test, respectively. By varying the number of *Fourier* components from $D = 1$ to $D = 5$, the optimal value was found to be $D = 4$. The corresponding coupling function $\tilde{H}(\Delta\theta)$ is shown by the solid red line in figure 4*c*. The estimated function is in good agreement with the one obtained by the convolution of averaged phase sensitivity function (figure 4*a*) and the averaged input waveform (figure 4*b*). Using the estimated phase equations, the synchronization diagram of the original two coupled Rössler equations can be recovered, where the onset of synchronization was predicted at $C = 0.042$, which is close to the real onset of $C = 0.04$ (figure 4*d*). This suggests that our simple method of estimating the coupling function provides a good approximation of describing the phase dynamics of phase-coherent chaotic oscillators.

(c) Application to circuit experiment

Finally, we apply our method to experimental data generated from the Van der Pol electric circuit [83] to demonstrate the performance of our method in a realistic experimental setting. As shown in figure 5*a*, the system is based on an LC circuit, composed of an inductor (L) and a capacitor (C_1). To form a negative-resistance converter, three positive resistors (R_1, R_2, R_3) were

Table 1. Parameters of Van der Pol circuit.

L	500 (mH)
C_1	2.2 (uF)
R_1	2.543 (KΩ)
R_2	62.7 (kΩ)
R_3	10 (kΩ)
V_{DD}	5 (V)
V_{SS}	−5 (V)
OPAMP	LF412CN
C_2	10 (nF)

connected to a voltage-controlled voltage source (i.e. operational amplifier and its associated power supplies V_{DD}, V_{SS}) [84]. External forcing $G(t)$ was injected from a function generator (Keysight 33500B) to the Van der Pol circuit through a capacitor (C_2). Physical parameters of the electric components used in the present experiment are summarized in table 1. To obtain the phase sensitivity function, 220 impulses (stimulus duration: $\tau = 380\,\mu s$, stimulus strength: $V = 3\,V$) were randomly injected as the external force $G(t)$. The circuit output as well as the input impulses were simultaneously measured with a sampling frequency of 12.5 kHz. First, the phase sensitivity function $\tilde{Z}$ was estimated by fitting the phase model (4.1) to the measured data with the multiple-shooting method. Natural frequency $f_n = 110.5\,\text{Hz}$ (i.e. $\omega = 2\pi f_n$), measured before the stimulus experiment, was used in the phase dynamics. The number of the *Fourier* components was set to $D = 4$. As shown in figure 5*b*, the estimated phase sensitivity $\tilde{Z}(\theta)$ fits to the experimental observation of phase response data well.

Next, a sinusoidal forcing $G(t) = V \sin(\Omega t)$ (forcing frequency: 106 Hz, forcing amplitude: $V = 0.6\,V$) was applied to the Van der Pol circuit. The circuit output as well as the forcing waveforms were simultaneously measured with a sampling frequency of 12.5 kHz. By the multiple-shooting method, which fits the phase equations (2.4) to the measured data, the coupling function $\tilde{H}$ (number of *Fourier* components: $D = 1$) was estimated. In figure 5*c*, the estimated coupling function is compared with the one obtained by the averaging of the phase sensitivity function $\tilde{Z}$, estimated from the impulse stimuli, and the input sine waveform $G(t)$. Despite a slight difference in the initial phase, the coupling functions agree quite well with each other. In figure 5*d*, the estimated phase equations recovered the synchronization diagram of the experimental system, where the onset of synchronization was predicted at $V = 0.73\,V$, which is very close to the real onset of $V = 7\,V$.

5. Discussions and conclusion

The multiple-shooting method has been focused on as a non-invasive approach to estimate coupling functions from multivariate time series measured from a real or synthetic complex dynamical system [31]. Among various methods developed so far [7,32–36,38–41], which are based on the Bayesian estimation and other variants, the multiple-shooting provides a straightforward approach to fit the phase equations to phase data measured from an oscillator network. Despite its simplicity, the method was shown to be capable of precisely estimating the coupling function of the coupled FHN oscillators including higher-harmonic terms. The estimation was found effective for a large network of up to 512 oscillators. Utilization of the transient part of data successfully enlarged applicability of the estimation technique even in a synchronized regime of coupled oscillators. The estimated coupling function was further applied to inference of network topology and chaotic phase synchrony. Precise estimation of the coupling functions was shown to improve the reconstruction of network topology. As another

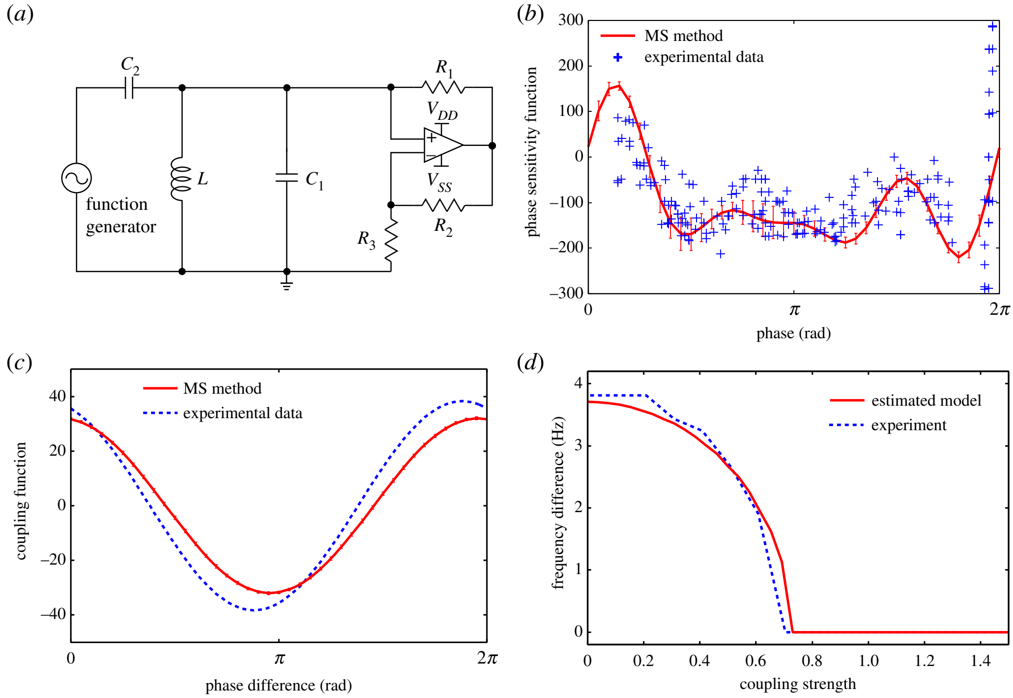

Figure 5. Experiment of Van der Pol oscillator circuit. (*a*) Schematic illustration of the Van der Pol circuit, that is composed of an inductor (L), a capacitor (C_1), three resistors (R_1, R_2, R_3), an operational amplifier, and its associated power supplies (V_{DD}, V_{SS}). External forcing is injected from a function generator (Keysight 33500B) through a capacitor (C_2). (*b*) Phase sensitivity function estimated by the multiple-shooting method (red line) and the perturbation experiment (crosses). (*c*) Coupling functions $\tilde{H}(\Delta\theta)$ estimated by the present method (solid red line) and one (dashed blue line) obtained by the averaging of the experimentally obtained phase sensitivity function and the sinusoidal input waveform. (*d*) Synchronization diagram of the estimated phase model (solid red line) and the experimental circuit system (dashed blue line). (Online version in colour.)

intriguing issue, estimation of the phase sensitivity function was also discussed. Although the phase sensitivity function obtained by deconvolution of the estimated coupling function was slightly deviated from the true function, refinement has been made by extending the multiple shooting method directly to the phase data of a driven limit cycle oscillator. Finally, efficiency of the present approach was demonstrated with the experimental data measured from the Van der Pol electric circuit with a sinusoidal forcing.

Beyond experimental systems in physics, chemistry and engineering, we foresee that our method will be applicable to systems of rhythmic, interacting elements such as cellular gene expressions in the suprachiasmatic nucleus (SCN) [56], electrical activities of cardiac pacemakers [57], inferior olive neurons in the cerebellum [85], and can give insights useful for domain-scientists in biology and neuroscience.

While considering our method of potentially practical use for various systems, its usefulness is not without limitations. The main among them is the assumption that the studied system can be approximated as a network of weakly coupled limit cycles [59]. This, however, is not true for all systems encountered in nature. For instance, in gene regulatory networks, phases of the clock component genes are tightly connected to each other [86]. It has been known that cortical neurons fire with a strong synchrony during epileptic seizure [87]. Such strongly coupled systems should be carefully distinguished and avoided as a target of modelling the phase dynamics. In the case that the system property is not well understood, it is non-trivial to judge only from the recorded data whether the coupling is weak enough to apply the phase modelling to the oscillator network. It is an important open problem to provide a criterion to assess whether the phase model is suitable for analysing the observed time series without prior knowledge on the underlying dynamical equations.

Another limitation is the length of the available time series: namely, experimental measurements, for a variety of realistic reasons, could produce the data (time series) of only a very short length. For instance, time resolved data on gene regulation are not likely to yield time series with much more than 10 cycles. In this case, our method might be of limited use. Also, realistic data are almost always noisy. The noise strength, depending on the experimental scenario, could be quite severe. Especially, the phase extraction process in our modelling is rather sensitive to noise. Temporal fluctuation and noise in natural frequencies of the oscillator elements may also cause estimation error in the coupling functions. In this respect, noise tolerance should be carefully examined, before the application to data contaminated with observational/dynamical noise.

Also, networks in the real world are large and only partials of the dynamics elements are observable. Although our method was shown to be robust against system size as far as the oscillator elements are uniformly connected and they are desynchronized with each other, the effect of unobserved oscillator states should be examined carefully. Heterogeneity and hierarchy in the coupling functions may require further extension of the present approach.

Finally, we conclude the paper with a brief discussion of how our method's performance compares to the performance of other methods that reconstruct coupling functions in oscillatory systems. Unfortunately, such comparison is not simple to make, since various available methods depart from very different hypotheses and knowledge about the system. Stronger hypotheses lead to better inferences, but the information on whether the hypotheses are met is not always available. This renders any independent comparison of reconstruction methods difficult. One could argue that methods aimed at only network topology are more useful and precise, but such methods neglect the entire dynamical nature of many real networks. On the other hand, certain methods give excellent results, but are limited to dynamical systems with specific properties. In fact, our method belongs to this category, since it assumes the limit cycle nature of the individual units. Furthermore, methods can be divided into invasive ones (that interfere with system's ongoing dynamics) and non-invasive ones (that do not). Again, their real merits are hard to compare, since invasive methods, although often non practical, will almost always give better results. Therefore, we here conclude that our reconstruction concept, although limited by the assumption of limit cycles, is a promising—and above all *practical*—approach implementable in real experiments.

Data accessibility. Experimental data generated from electric circuit are available in Dryad dataset (https://doi.org/10.5061/dryad.z34tmpg80).

Authors' contributions. I.T.T. designed the study and performed the numerical simulations and the data analysis. K.I. carried out the circuit experiments. I.T.T. and Z.L. wrote the manuscript. All authors read and approved the manuscript.

Competing interests. We declare we have no competing interests.

Funding. I.T.T. acknowledges support by Grant-in-Aid for Scientific Research (grant nos. 17H06313, 16H04848, 16K00343 and 18H02477) from Japan Society for the Promotion of Science (JSPS). Z.L. acknowledges support by EU via H2020-MSCA-ITN-2015 COSMOS 642563, and by Slovenian research agency via P1-0383 and J5-8236.

References

1. Newman M. 2007 *Networks, an introduction*. Oxford, UK: Oxford University Press.
2. Estrada E. 2011 *The structure of complex networks: theory and applications*. Oxford, UK: Oxford University Press.
3. Porter M, Gleeson J. 2016 *Dynamical systems on networks*. Berlin, Germany: Springer.
4. Barabasi AL. 2016 *Network science*. Cambridge, UK: Cambridge University Press.
5. Easley D, Kleinberg J. 2012 *Networks, crowds, and markets: reasoning about a highly connected world*. Cambridge, UK: Cambridge University Press.

6. Boccaletti S, Bianconi G, Criado R, Del Genio CI, Gómez-Gardenes J, Romance M, Sendina-Nadal I, Wang Z, Zanin M. 2014 The structure and dynamics of multilayer networks. *Phys. Rep.* **544**, 1–122. (doi:10.1016/j.physrep.2014.07.001)
7. Blaha KA, Pikovsky A, Rosenblum M, Clark MT, Rusin CG, Hudson JL. 2011 Reconstruction of two-dimensional phase dynamics from experiments on coupled oscillators. *Phys. Rev. E* **84**, 046201. (doi:10.1103/PhysRevE.84.046201)
8. Levnajić Z, Pikovsky A. 2011 Network reconstruction from random phase resetting. *Phys. Rev. Lett.* **107**, 034101. (doi:10.1103/PhysRevLett.107.034101)
9. Wang WX, Yang R, Lai YC, Kovanis V, Harrison MAF. 2011 Time-series–based prediction of complex oscillator networks via compressive sensing. *Europhys. Lett.* **94**, 48006. (doi:10.1209/0295-5075/94/48006)
10. Stankovski T, Duggento A, McClintock PV, Stefanovska A. 2012 Inference of time-evolving coupled dynamical systems in the presence of noise. *Phys. Rev. Lett.* **109**, 024101. (doi:10.1103/PhysRevLett.109.024101)
11. Kralemann B, Pikovsky A, Rosenblum M. 2014 Reconstructing effective phase connectivity of oscillator networks from observations. *New J. Phys.* **16**, 085013. (doi:10.1088/1367-2630/16/8/085013)
12. Levnajić Z, Pikovsky A. 2014 Untangling complex dynamical systems via derivative-variable correlations. *Sci. Rep.* **4**, 5030. (doi:10.1038/srep05030)
13. Timme M, Casadiego J. 2014 Revealing networks from dynamics: an introduction. *J. Phys. A: Math. Theor.* **47**, 343001. (doi:10.1088/1751-8113/47/34/343001)
14. Han X, Shen Z, Wang WX, Di Z. 2015 Robust reconstruction of complex networks from sparse data. *Phys. Rev. Lett.* **114**, 028701. (doi:10.1103/PhysRevLett.114.028701)
15. Nitzan M, Casadiego J, Timme M. 2017 Revealing physical network interactions from statistics of collective dynamics. *Sci. Adv.* **3**, e1600396. (doi:10.1126/sciadv.1600396)
16. Wang WX, Lai YC, Grebogi C. 2016 Data based identification and prediction of nonlinear and complex dynamical systems. *Phys. Rep.* **644**, 1–76. (doi:10.1016/j.physrep.2016.06.004)
17. Leguia MG, Andrzejak RG, Levnajić Z. 2017 Evolutionary optimization of network reconstruction from derivative-variable correlations. *J. Phys. A: Math. Theor.* **50**, 334001. (doi:10.1088/1751-8121/aa7925)
18. Rosenblum M *et al.* 2017 Reconstructing networks of pulse-coupled oscillators from spike trains. *Phys. Rev. E* **96**, 012209. (doi:10.1103/PhysRevE.96.012209)
19. Simidjievski N, Tanevski J, Ženko B, Levnajić Z, Todorovski L, Džeroski S. 2018 Decoupling approximation robustly reconstructs directed dynamical networks. *New J. Phys.* **20**, 113003. (doi:10.1088/1367-2630/aae941)
20. Papana A, Kyrtsou C, Kugiumtzis D, Diks C. 2013 Simulation study of direct causality measures in multivariate time series. *Entropy* **15**, 2635–2661. (doi:10.3390/e15072635)
21. Koutlis C, Kugiumtzis D. 2016 Discrimination of coupling structures using causality networks from multivariate time series. *Chaos* **26**, 093120. (doi:10.1063/1.4963175)
22. Zanin M, Papo D, Sousa PA, Menasalvas E, Nicchi A, Kubik E, Boccaletti S. 2016 Combining complex networks and data mining: why and how. *Phys. Rep.* **635**, 1–44. (doi:10.1016/j.physrep.2016.04.005)
23. Bridewell W, Langley P, Todorovski L, Džeroski S. 2008 Inductive process modeling. *Mach. Learn.* **71**, 1–32. (doi:10.1007/s10994-007-5042-6)
24. Džeroski S, Todorovski L. 2008 Equation discovery for systems biology: finding the structure and dynamics of biological networks from time course data. *Curr. Opin Biotechnol.* **19**, 360–368. (doi:10.1016/j.copbio.2008.07.002)
25. Schmidt M, Lipson H. 2009 Distilling free-form natural laws from experimental data. *Science* **324**, 81–85. (doi:10.1126/science.1165893)
26. Brunton SL, Proctor JL, Kutz JN. 2016 Discovering governing equations from data by sparse identification of nonlinear dynamical systems. *Proc. Natl Acad. Sci. USA* **113**, 3932–3937. (doi:10.1073/pnas.1517384113)
27. Simidjievski N, Todorovski L, Džeroski S. 2016 Modeling dynamic systems with efficient ensembles of process-based models. *PLoS ONE* **11**, e0153507. (doi:10.1371/journal.pone.0153507)

28. Tanevski J, Todorovski L, Džeroski S. 2016 Learning stochastic process-based models of dynamical systems from knowledge and data. *BMC Syst. Biol.* **10**, 30. (doi:10.1186/s12918-016-0273-4)
29. Tanevski J, Todorovski L, Džeroski S. 2016 Process-based design of dynamical biological systems. *Sci. Rep.* **6**, 34107. (doi:10.1038/srep34107)
30. Čerepnalkoski D, Taškova K, Todorovski L, Atanasova N, Džeroski S. 2012 The influence of parameter fitting methods on model structure selection in automated modeling of aquatic ecosystems. *Ecol. Modell* **245**, 136–165. (doi:10.1016/j.ecolmodel.2012.06.001)
31. Tokuda IT, Jain S, Kiss IZ, Hudson JL. 2007 Inferring phase equations from multivariate time series. *Phys. Rev. Lett.* **99**, 064101. (doi:10.1103/PhysRevLett.99.064101)
32. Kralemann B, Cimponeriu L, Rosenblum M, Pikovsky A, Mrowka R. 2007 Uncovering interaction of coupled oscillators from data. *Phys. Rev. E* **76**, 055201. (doi:10.1103/PhysRevE.76.055201)
33. Kralemann B, Cimponeriu L, Rosenblum M, Pikovsky A, Mrowka R. 2008 Phase dynamics of coupled oscillators reconstructed from data. *Phys. Rev. E* **77**, 066205. (doi:10.1103/PhysRevE.77.066205)
34. Cadieu CF, Koepsell K. 2010 Phase coupling estimation from multivariate phase statistics. *Neural Comput.* **22**, 3107–3126. (doi:10.1162/NECO_a_00048)
35. Kralemann B, Pikovsky A, Rosenblum M. 2011 Reconstructing phase dynamics of oscillator networks. *Chaos* **21**, 025104. (doi:10.1063/1.3597647)
36. Zhu Y, Hsieh YH, Dhingra RR, Dick TE, Jacono FJ, Galán RF. 2013 Quantifying interactions between real oscillators with information theory and phase models: application to cardiorespiratory coupling. *Phys. Rev. E* **87**, 022709. (doi:10.1103/PhysRevE.87.022709)
37. Pikovsky A. 2018 Reconstruction of a random phase dynamics network from observations. *Phys. Lett. A* **382**, 147–152. (doi:10.1016/j.physleta.2017.11.012)
38. Suzuki K, Aoyagi T, Kitano K. 2018 Bayesian estimation of phase dynamics based on partially sampled spikes generated by realistic model neurons. *Front. Comput. Neurosci.* **11**, 116. (doi:10.3389/fncom.2017.00116)
39. Miyazaki J, Kinoshita S. 2006 Determination of a coupling function in multicoupled oscillators. *Phys. Rev. Lett.* **96**, 194101. (doi:10.1103/PhysRevLett.96.194101)
40. Tokuda IT, Wagemakers A, Sanjuán MA. 2010 Predicting the synchronization of a network of electronic repressilators. *Int. J. Bifurcation Chaos* **20**, 1751–1760. (doi:10.1142/S0218127410026800)
41. Stankovski T, Pereira T, McClintock PV, Stefanovska A. 2017 Coupling functions: universal insights into dynamical interaction mechanisms. *Rev. Mod. Phys.* **89**, 045001. (doi:10.1103/RevModPhys.89.045001)
42. Kiss IZ, Zhai Y, Hudson JL. 2005 Predicting mutual entrainment of oscillators with experiment-based phase models. *Phys. Rev. Lett.* **94**, 248301. (doi:10.1103/PhysRevLett.94.248301)
43. Galán RF, Ermentrout GB, Urban NN. 2005 Efficient estimation of phase-resetting curves in real neurons and its significance for neural-network modeling. *Phys. Rev. Lett.* **94**, 158101. (doi:10.1103/PhysRevLett.94.158101)
44. Ota K, Omori T, Aonishi T. 2009 Map estimation algorithm for phase response curves based on analysis of the observation process. *J. Comput. Neurosci.* **26**, 185–202. (doi:10.1007/s10827-008-0104-8)
45. Nakae K, Iba Y, Tsubo Y, Fukai T, Aoyagi T. 2010 Bayesian estimation of phase response curves. *Neural Netw.* **23**, 752–763. (doi:10.1016/j.neunet.2010.04.002)
46. Hong S, Robberechts Q, Schutter ED. 2012 Efficient estimation of phase-response curves via compressive sensing. *J. Neurophysiol.* **108**, 2069–2081. (doi:10.1152/jn.00919.2011)
47. Goldberg JA, Atherton JF, Surmeier DJ. 2013 Spectral reconstruction of phase response curves reveals the synchronization properties of mouse globus pallidus neurons. *J. Neurophysiol.* **110**, 2497–2506. (doi:10.1152/jn.00177.2013)
48. Saifee TA, Edwards MJ, Kassavetis P, Gilbertson T. 2015 Estimation of the phase response curve from parkinsonian tremor. *J. Neurophysiol.* **115**, 310–323. (doi:10.1152/jn.00216.2015)
49. Imai T, Ota K, Aoyagi T. 2017 Robust measurements of phase response curves realized via multicycle weighted spike-triggered averages. *J. Phys. Soc. Jpn.* **86**, 024009. (doi:10.7566/JPSJ.86.024009)

50. Cestnik R, Rosenblum M. 2018 Inferring the phase response curve from observation of a continuously perturbed oscillator. *Sci. Rep.* **8**, 13606. (doi:10.1038/s41598-018-32069-y)
51. Okada M, Kaburagi T, Tokuda IT. 2019 Acoustic measurements of the infinitesimal phase response curve from a sounding organ pipe. *Phys. Lett. A* **383**, 1733–1741. (doi:10.1016/j.physleta.2019.02.034)
52. Nakae K. 2019 Statistical estimation of phase response curves using data transformation. *J. Phys. Soc. Jpn.* **88**, 084003. (doi:10.7566/JPSJ.88.084003)
53. Tokuda IT, Wickramasinghe M, Kiss IZ. 2013 Detecting connectivity of small, dense oscillator networks from dynamical measurements based on a phase modeling approach. *Phys. Lett. A* **377**, 1862–1867. (doi:10.1016/j.physleta.2013.05.016)
54. Baake E, Baake M, Bock H, Briggs K. 1992 Fitting ordinary differential equations to chaotic data. *Phys. Rev. A* **45**, 5524–5529. (doi:10.1103/PhysRevA.45.5524)
55. Press WH, Teukolsky SA, Vetterling WT, Flannery BP. 2007 *Numerical recipes 3rd edition: the art of scientific computing*. Cambridge, UK: Cambridge University Press.
56. Yamaguchi S, Isejima H, Matsuo T, Okura R, Yagita K, Kobayashi M, Okamura Hs. 2003 Synchronization of cellular clocks in the Suprachiasmatic nucleus. *Science* **302**, 1408–1412. (doi:10.1126/science.1089287)
57. Verheijck EE, Wilders R, Joyner RW, Golod DA, Kumar R, Jongsma HJ, Bouman LN, van Ginneken AC. 1998 Pacemaker synchronization of electrically coupled rabbit sinoatrial node cells. *J. Gen. Physiol.* **111**, 95–112. (doi:10.1085/jgp.111.1.95)
58. Winfree AT. 2001 *The geometry of biological time*. New York, NY: Springer.
59. Kuramoto Y. 1984 *Chemical oscillations, waves, and turbulence*. Berlin, Germany: Springer.
60. Pikovsky A, Rosenblum M, Kurths J. 2003 *Synchronization: a universal concept in nonlinear sciences*, vol. 12. Cambridge, UK: Cambridge University Press.
61. Acebrón JA, Bonilla LL, Vicente CJP, Ritort F, Spigler R. 2005 The kuramoto model: a simple paradigm for synchronization phenomena. *Rev. Mod. Phys.* **77**, 137–185. (doi:10.1103/RevModPhys.77.137)
62. Stone M. 1977 An asymptotic equivalence of choice of model by cross-validation and Akaike's criterion. *J. R. Stat. Soc. B (Methodol.)* **39**, 44–47. (doi:10.1111/j.2517-6161.1977.tb01603.x)
63. FitzHugh R. 1961 Impulses and physiological states in theoretical models of nerve membrane. *Biophys. J.* **1**, 445–466. (doi:10.1016/S0006-3495(61)86902-6)
64. Nagumo J, Arimoto S, Yoshizawa S. 1962 An active pulse transmission line simulating nerve axon. *Proc. IRE* **50**, 2061–2070. (doi:10.1109/JRPROC.1962.288235)
65. Ermentrout B. 1996 Type I membranes, phase resetting curves, and synchrony. *Neural Comput.* **8**, 979–1001. (doi:10.1162/neco.1996.8.5.979)
66. Horbelt W, Timmer J, Bünner M, Meucci R, Ciofini M. 2001 Identifying physical properties of a CO_2 laser by dynamical modeling of measured time series. *Phys. Rev. E* **64**, 016222. (doi:10.1103/PhysRevE.64.016222)
67. Schreiber T. 2000 Measuring information transfer. *Phys. Rev. Lett.* **85**, 461–464. (doi:10.1103/PhysRevLett.85.461)
68. Rosenblum MG, Pikovsky AS. 2001 Detecting direction of coupling in interacting oscillators. *Phys. Rev. E* **64**, 045202. (doi:10.1103/PhysRevE.64.045202)
69. Romano MC, Thiel M, Kurths J, Grebogi C. 2007 Estimation of the direction of the coupling by conditional probabilities of recurrence. *Phys. Rev. E* **76**, 036211. (doi:10.1103/PhysRevE.76.036211)
70. Hempel S, Koseska A, Kurths J, Nikoloski Z. 2011 Inner composition alignment for inferring directed networks from short time series. *Phys. Rev. Lett.* **107**, 054101. (doi:10.1103/PhysRevLett.107.054101)
71. Schelter B, Winterhalder M, Dahlhaus R, Kurths J, Timmer J. 2006 Partial phase synchronization for multivariate synchronizing systems. *Phys. Rev. Lett.* **96**, 208103. (doi:10.1103/PhysRevLett.96.208103)
72. Nawrath J, Romano MC, Thiel M, Kiss IZ, Wickramasinghe M, Timmer J, Kurths J, Schelter B. 2010 Distinguishing direct from indirect interactions in oscillatory networks with multiple time scales. *Phys. Rev. Lett.* **104**, 038701. (doi:10.1103/PhysRevLett.104.038701)
73. Wickramasinghe M, Kiss IZ. 2011 Phase synchronization of three locally coupled chaotic electrochemical oscillators: Enhanced phase diffusion and identification of indirect coupling. *Phys. Rev. E* **83**, 016210. (doi:10.1103/PhysRevE.83.016210)

74. Runge J, Heitzig J, Petoukhov V, Kurths J. 2012 Escaping the curse of dimensionality in estimating multivariate transfer entropy. *Phys. Rev. Lett.* **108**, 258701. (doi:10.1103/PhysRevLett.108.258701)
75. Timme M. 2007 Revealing network connectivity from response dynamics. *Phys. Rev. Lett.* **98**, 224101. (doi:10.1103/PhysRevLett.98.224101)
76. Stankovski T, Ticcinelli V, McClintock PV, Stefanovska A. 2015 Coupling functions in networks of oscillators. *New J. Phys.* **17**, 035002. (doi:10.1088/1367-2630/17/3/035002)
77. Stankovski T, Petkoski S, Raeder J, Smith AF, McClintock PV, Stefanovska A. 2016 Alterations in the coupling functions between cortical and cardio-respiratory oscillations due to anaesthesia with propofol and sevoflurane. *Phil. Trans. R. Soc. A* **374**, 20150186. (doi:10.1098/rsta.2015.0186)
78. Stankovski T, Ticcinelli V, McClintock PV, Stefanovska A. 2017 Neural cross-frequency coupling functions. *Front. Syst. Neurosci.* **11**, 33. (doi:10.3389/fnsys.2017.00033)
79. Kralemann B, Pikovsky A, Rosenblum M. 2013 Detecting triplet locking by triplet synchronization indices. *Phys. Rev. E* **87**, 052904. (doi:10.1103/PhysRevE.87.052904)
80. Wiener N. 1949 *Extrapolation, interpolation, and smoothing of stationary time series: with engineering applications*. Cambridge, MA: MIT Press.
81. Rosenblum MG, Pikovsky AS, Kurths J. 1996 Phase synchronization of chaotic oscillators. *Phys. Rev. Lett.* **76**, 1804–1807. (doi:10.1103/PhysRevLett.76.1804)
82. Rössler OE. 1976 An equation for continuous chaos. *Phys. Lett. A* **57**, 397–398. (doi:10.1016/0375-9601(76)90101-8)
83. Van der Pol B, Van Der Mark J. 1927 Frequency demultiplication. *Nature* **120**, 363–364. (doi:10.1038/120363a0)
84. Kennedy MP. 1992 Robust op amp realization of Chua's circuit. *Frequenz* **46**, 66–80. (doi:10.1515/FREQ.1992.46.3-4.66)
85. Tokuda IT, Hoang H, Kawato M. 2017 New insights into olivo-cerebellar circuits for learning from a small training sample. *Curr. Opin. Neurobiol.* **46**, 58–67. (doi:10.1016/j.conb.2017.07.010)
86. Zhang R, Lahens NF, Ballance HI, Hughes ME, Hogenesch JB. 2014 A circadian gene expression atlas in mammals: implications for biology and medicine. *Proc. Natl Acad. Sci. USA* **111**, 16 219–16 224. (doi:10.1073/pnas.1408886111)
87. Velazquez JLP, Carlen PL. 2000 Gap junctions, synchrony and seizures. *Trends Neurosci.* **23**, 68–74. (doi:10.1016/S0166-2236(99)01497-6)